

# Large-scale Point Cloud Registration Based on Graph Matching Optimization

Qianliang Wu\*, Yaqi Shen\*, Guofeng Mei, Yaqing Ding, Lei Luo, Jin Xie†, Jian Yang†

**Abstract**—Point Clouds Registration is a fundamental and challenging problem in 3D computer vision. It has been shown that the isometric transformation is an essential property in rigid point cloud registration, but the existing methods only utilize it in the outlier rejection stage. In this paper, we emphasize that the isometric transformation is also important in the feature learning stage for improving registration quality. We propose a **Graph Matching Optimization based Network** (denoted as **GMONet** for short), which utilizes the graph matching method to explicitly exert the isometry preserving constraints in the point feature learning stage to improve the point representation. Specifically, we exploit the partial graph matching constraint to enhance the overlap region detection abilities of super points (*i.e.*, down-sampled key points) and full graph matching to refine the registration accuracy at the fine-level overlap region. Meanwhile, we leverage the mini-batch sampling to improve the efficiency of the full graph matching optimization. Given high discriminative point features in the evaluation stage, we utilize the RANSAC approach to estimate the transformation between the scanned pairs. The proposed method has been evaluated on the 3DMatch/3DLoMatch benchmarks and the KITTI benchmark. The experimental results show that our method achieves competitive performance compared with the existing state-of-the-art baselines.

## I. INTRODUCTION

Point Cloud Registration is a fundamental problem in numerous computer vision applications, such as 3D reconstruction [1]–[3], localization [4]–[6], and pose estimation [7], [8], etc. The goal of point cloud registration is to estimate the rigid transformation between two scans. However, due to viewpoint change or occlusion in real-world sensor data, the partial overlap registration of point cloud is still a challenging problem.

Recent popular deep Point Cloud Registration methods are mainly divided into two categories: feature-matching-based methods [9]–[15] and outlier-rejection-based methods [16]–[20]. The outlier-rejection-based methods depend on the candidate correspondences computed by the point features extracted from the pre-train models (*e.g.*, FCGF [10]), where these candidate correspondences may lose the most wanted correspondences after the filtering operation

Qianliang Wu, Yaqi Shen, Yaqing Ding, Lei Luo, Jin Xie, Jian Yang are with PCA Lab, Key Lab of Intelligent Perception and Systems for High-Dimensional Information of Ministry of Education, and Jiangsu Key Lab of Image and Video Understanding for Social Security, School of Computer Science and Engineering, Nanjing University of Science and Technology.

Guofeng Mei is with the Faculty of Engineering and Information Technology, University of Technology Sydney, Sydney NSW 2007, Australia.

E-mail:{wuqianliang, syq, dingyaqing, csjxie, csjyayang}@njjust.edu.cn, luoleipitt@gmail.com, guofeng.mei@student.uts.edu.au

† Corresponding authors: Jin Xie, Jian Yang

\* Equal contributions

(*e.g.* KNN searching in feature space). The feature-matching-based methods mainly emphasize learning more discriminative point features. Some state-of-the-art feature-matching-based methods have tried to enhance the local features by adding translation-invariant [9], [12] and rotation-invariant embeddings [14], [15], [21]. To capture the global spatial information (*e.g.*, global contextual information of the overlap region), [12]–[14], [22] leverage the Transformer [23] to get the global structural information. Specifically, [14] embeds the pair-wise distance and local triplet angles into the self-attention operator to obtain strong rotation-invariant features. Moreover, [13], [14] adopt a point-to-patch grouping strategy and utilize the optimal transport to correct the point correspondences in local patch pairs. However, this first-order (*i.e.*, point-to-point) local patch-to-patch matching strategy ignores the second-order (*i.e.*, edge-to-edge) constraint about isometric transformation. To this end, we emphasize that the explicit second-order constraint should be injected into the point feature learning stage to enhance the ability of the point features to capture the global structure information of spatial consistency.

We propose **Graph Matching Optimization based Network** (denoted as **GMONet** for short), incorporating the KP-Conv [11] as our feature backbone network. Inspired by [17], [18], [24], [25], we explicitly deploy graph matching to characterize second-order spatial consistency and integrate it into the feature learning stage. At the coarse level, we downsample the points to super points (sparse key points) and utilize the geometric attention layer [14] to generate super point features. Then, we deploy the partial graph matching to classify whether super points are in the overlap region. The partial graph matching constraint on super points can enhance the ability to capture global second-order spatial consistency. To solve the partial graph matching optimization, we transform it into an  $\epsilon$ -convex optimal transport problem by using the proximal point method [26]–[28]. We also utilize the inexact proximal point method [29] to improve efficiency. At the fine level, we first use skip links and unary layers to recover the fine-level points and features from super points features. Next, we use the graph matching optimization to correct the correspondences in overlap regions of point cloud pairs. We also apply mini-batch optimal transport [30] strategy to accelerate the computing speed. Two level graph matching layers are based on a global, fully-connected graph structure. They can capture long-range spatial consistency constraints. We advocate that if the point features have learned enough global structure information, the solution of optimization graph matching should be consistent with the ground truth

correspondences.

Our main contributions can be summarized as follows:

- To our knowledge, we are the first to consider graph matching optimization in the feature learning stage for large scale point cloud registration problem. Specifically, we apply partial graph matching constraints on coarse-level super points and full graph matching constraint in the overlap region of the fine-level points.
- We use the mini-batch technique to solve the graph matching optimization in the overlap regions, which makes it applicable in a large-scale point cloud. We propose a new accelerated graduated non-convexity solver to solve Koopmans-Beckmann’s QAP for point correspondences in overlap regions.
- We exploit the inexact proximal point method to solve the partial graph matching problem to reduce the complexity and guarantee convergence.

## II. RELATED WORK

### A. Traditional Methods

ICP [31] is a classical local registration method that iteratively computes the point correspondences and optimizes the least-square problem of transformation. The drawback of ICP is that it needs a good initialization to prevent the locally optimal estimation. To optimize globally, GO-ICP [32] utilizes branch-and-bound optimization. However, this method is sensitive to outliers. By introducing a robust estimator (*e.g.*, Geman-McClure), FGR [33] improves the robustness against the outliers. Also, Teaser [6] leverages another robust estimator (*i.e.*, Truncated Least Squares (TLS)) and max clique to filter the inlier correspondences.

### B. Feature-Matching-Based Methods

The famous 3DMatch [34] first extracts multi-view local patch and their voxel grid of Truncated Distance Function (TDF) values, then learns 3D feature descriptors in a metric learning way. PPFNet [35] uses Point Pair Features to encode local patches as inputs of the PointNet network and learns the point features by N-tuple loss. FCGF [10] designs a fully-convolutional network to compute geometric features in a single pass, which achieves a faster accurate feature extraction speed. The unsupervised PPF-FoldNet [36] and CapsuleNet [37] exploit an encoder-decoder network to learn local feature descriptors based on point cloud reconstruction. D3feat [9] and Predator [12] utilize a KPConv [11] module to learn translation-invariant point features. Based on Predator, CoFiNet [13] uses Sinkhorn’s algorithm [38] to solve the optimal transport problem to get an optimal solution based on the initial correspondence proposal. Furthermore, Geo-Transformer [14] proposes to add edge-distance and local triplet angle into the self-attention layer to learn rotation-invariant embeddings. The RGM [39] utilize a graph feature extractor network to compute the soft correspondence matrix and convert it to hard correspondence matrix by using LAP solver. However, the LAP solver based on Hungarian algorithm [40] prevent it from applying on large scale point cloud problem.

### C. Learning-based Outlier Rejection Methods

Another class of deep learning methods focuses on the outlier rejection stage after getting the initial correspondences built from the point feature backbone. DGR [41] and 3DRegnet [42] use a convolutional network and differentiable Weighted Procrustes solver to classify the inlier/outlier correspondences. [19] generates a candidate matching map with the Dynamic Graph CNN (DGCNN) [43] and refines it with neighborhood consensus to predict pseudo-matching points. CEMNet [20] utilizes the differentiable Cross-Entropy Method [44] to filter reliable inlier correspondences. PointDSC [17] treats correspondence as points, uses max clique to get the potential high confidence inlier correspondence as key points, and conducts a one-shot max consensus to get the most confident correspondences. DHVR [45] uses the Hough Voting to discover the best transformation in 6D sparse Hough space of transformation parameters. The other concurrent work COTReg [18] which is a outlier rejection method utilizes an unbalanced optimal transport layer to compute reliable correspondences for point cloud registration.

### D. Graph Matching Methods

Since the graph matching problem [24], [46] can model point-wise, pair-wise, and even more, higher order [47] similarities between point sets, more and more researchers [48]–[54] consider this method in image matching or network alignment problems. The classical solver for graph matching is the Frank-Wolfe’s algorithm [55] under the Convex-Concave Relaxation [56]. The other way is to add an entropic regularized item to the objective function to convert it to an  $\epsilon$ -convex problem which can be easily solved by the project gradient descent [26], [27]. In order to use graph matching (or optimal transport) in large-scale problems, researchers propose the mini-batch OT (Optimal Transport) [57], mini-batch UOT (Unbalanced Optimal Transport) [58], and mini-batch POT (Partial Optimal Transport) [30] methods to improve efficiency while guaranteeing accuracy.

## III. METHOD

### A. Problem Formulation

Give two unordered point clouds  $\mathbf{P} = \{\mathbf{p}_i \in \mathbb{R}^3 | i = 1 \dots N\}$  and  $\mathbf{Q} = \{\mathbf{q}_i \in \mathbb{R}^3 | i = 1 \dots M\}$ , where  $N$  and  $M$  are the different number of points (suppose  $M > N$ ), the goal of the point cloud registration is to recover the rigid transformation  $\mathbf{T}$  consisting of  $\mathbf{R} \in SO(3)$  and  $\mathbf{t} \in \mathbb{R}^3$  that aligns  $\mathbf{P}$  to  $\mathbf{Q}$ . We focus on the partial overlap point cloud registration problem [12]. In this case, after applying the ground-truth transformation  $\mathbf{T}$ , the overlap ratio of aligned  $\mathbf{P}$  and  $\mathbf{Q}$  is above a certain threshold  $\tau$ :

$$|\{\mathbf{p}_i | \mathbf{p}_i \in \mathbf{P} \wedge \|\mathbf{T}(\mathbf{p}_i) - \mathbf{NN}(\mathbf{T}(\mathbf{p}_i), \mathbf{Q})\|_2 \leq v\}| / |\mathbf{P}| > \tau, \quad (1)$$

where  $|\cdot|$  is the set cardinality,  $\|\cdot\|_2$  is the Euclidean norm,  $\mathbf{NN}$  is the nearest-neighbor operator, and  $v$  is a radius that depends on the point density. The overlap ratio  $\tau$  is typically greater than 30% in 3DMatch [34] and greater than 10% for low-overlap 3DLoMatch [12].

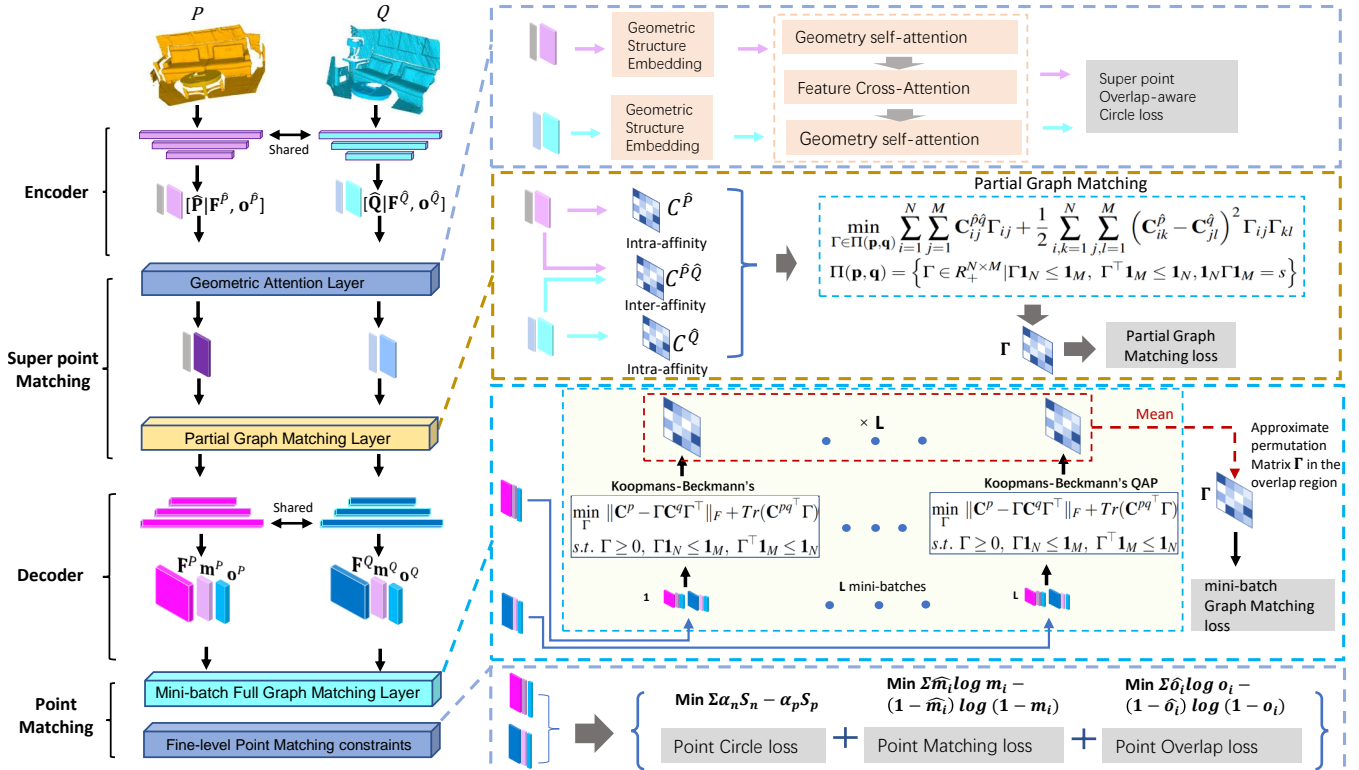


Fig. 1. Network overview of our proposed GMONet. First, the point clouds  $\mathbf{P}$  and  $\mathbf{Q}$  are fed to the down-sampling encoder and attention layers to obtain the super point  $(\hat{\mathbf{P}}, \hat{\mathbf{Q}})$ , and their features  $(\mathbf{F}^{\hat{\mathbf{P}}}, \mathbf{F}^{\hat{\mathbf{Q}}})$ , overlap scores  $(\mathbf{o}^{\hat{\mathbf{P}}}, \mathbf{o}^{\hat{\mathbf{Q}}})$ , and global matching scores  $(\mathbf{m}^{\hat{\mathbf{P}}}, \mathbf{m}^{\hat{\mathbf{Q}}})$ . Then, we apply the partial graph matching constraint on super points to improve the overlap region detection. Next, we use three upsampling layers to recover the fine-level points, and their features  $(\mathbf{F}^{\mathbf{P}}, \mathbf{F}^{\mathbf{Q}})$ , overlap scores  $(\mathbf{o}^{\mathbf{P}}, \mathbf{o}^{\mathbf{Q}})$ , and global matching scores  $(\mathbf{m}^{\mathbf{P}}, \mathbf{m}^{\mathbf{Q}})$ . Lastly, a mini-batch graph matching constraint is applied on the fine-level points in the overlap region to refine the global matching scores.

## B. Method overview

The structure of our framework is illustrated in Fig.1. We choose KPCConv [11] as our feature backbone. Firstly, one point feature encoder consisting of three subsampling layers is used to downsample the given point cloud pairs to the sparse super points (*i.e.*,  $\hat{\mathbf{P}} \in \mathbb{R}^{N' \times 3}$  and  $\hat{\mathbf{Q}} \in \mathbb{R}^{M' \times 3}$ ) and extracts associated features. Then we utilize the geometric attention layer (see section III-C.2) to encode the super points to get rotation-invariant embeddings (*i.e.*,  $\mathbf{F}^{\hat{\mathbf{P}}} \in \mathbb{R}^{N' \times b}$  and  $\mathbf{F}^{\hat{\mathbf{Q}}} \in \mathbb{R}^{M' \times b}$ ) and compute their overlap scores and matching scores (*i.e.*,  $\mathbf{o}^{\hat{\mathbf{P}}}$ ,  $\mathbf{o}^{\hat{\mathbf{Q}}}$  and  $\mathbf{m}^{\hat{\mathbf{P}}}$ ,  $\mathbf{m}^{\hat{\mathbf{Q}}}$ ) through several linear layers. After that, we deploy a partial graph matching constraint to enhance the super points' ability to detect overlap regions (see section III-D). Next, we use a decoder that consisting of three upsampling layers to decode the fine-level points and their corresponding features (*i.e.*,  $\mathbf{F}^{\mathbf{P}} \in \mathbb{R}^{N \times 32}$  and  $\mathbf{F}^{\mathbf{Q}} \in \mathbb{R}^{N \times 32}$ ), overlapping scores (*i.e.*,  $\mathbf{o}^{\mathbf{P}}$  and  $\mathbf{o}^{\mathbf{Q}}$ ), and global matching scores (*i.e.*,  $\mathbf{m}^{\mathbf{P}}$  and  $\mathbf{m}^{\mathbf{Q}}$ ). Lastly, we take the mini-batch uniform sampling to get several subsets from overlap region and use full graph matching in each subset to refine the whole of overlap regions' matching score from global scope (see section III-E). Since the KPCConv [11] backbone and geometric attention layer [14], [59] are commonly used in the state-of-the-art methods, we do not retell them in our paper and primarily describe our two main contributed modules in the following sections.

## C. Point Feature Embedding

1) *Point Feature Encoder*: We follow [12] [13] to utilize the Kernel Point Convolution (KPCConv) [11] as the backbone for point feature extraction. Firstly, by three shared voxel-grid layers, raw point clouds are down sampled to super points  $\hat{\mathbf{P}} \in \mathbb{R}^{N' \times 3}$  and  $\hat{\mathbf{Q}} \in \mathbb{R}^{M' \times 3}$  and generated associated features  $\mathbf{F}^{\hat{\mathbf{P}}} \in \mathbb{R}^{N' \times b}$  and  $\mathbf{F}^{\hat{\mathbf{Q}}} \in \mathbb{R}^{M' \times b}$ .

2) *Geometric attention layer*: For super point embedding, we utilize the geometric transformer layer [14]. It encodes the local geometric structure embedding consisting of pairwise distance (*i.e.*, edge) and local triplet-wise angle in self attention. It also use cross-attention to do inter-point-cloud information exchange for overlap detection.

Local geometric structure embedding: For two points  $p_i$  and  $p_j$  in  $\hat{\mathbf{P}}$ , the point-wise distance is  $\delta_{ij} = \|p_i - p_j\|_2$ . To embedding the angle, we select the  $k$  nearest neighbors  $\kappa_i$  for  $p_i$ . For each  $\tilde{p}_x \in \kappa_i$ , the triplet-wise angle is computed as  $\rho_{i,j}^x = \angle(\Delta_{x,i}, \Delta_{j,i})$ , where  $\Delta_{j,i} := \mathbf{p}_j - \mathbf{p}_i$ . We define the geometric structure embedding as combination of the point-wise distance embedding and triplet-wise angle embedding:

$$\mathbf{r}_{i,j} = \mathbf{r}_{i,j}^D \mathbf{W}^D + \max_x (\mathbf{r}_{i,j,x}^A \mathbf{W}^A), \quad (2)$$

where  $\mathbf{r}_{i,j}^D$  and  $\mathbf{r}_{i,j,x}^A$  are computed with a sinusoidal function on  $\delta_{ij}/\sigma_d$  and  $\rho_{i,j}^x/\sigma_a$ .  $\sigma_d$  and  $\sigma_a$  are parameters to control the sensitivity to variations of distance and angle.  $\mathbf{W}^D, \mathbf{W}^A \in \mathbb{R}^{b \times b}$  are two linear projection layers. For points in  $\hat{\mathbf{Q}}$ , the

embeddings are computed in the same way.

**Self-attention and Cross-attention:** Given the super points' features and geometric structure embedding, we define the following geometric-aware self-attention:

$$a_{i,j} = \text{softmax} \left( \left[ \frac{(\mathbf{x}_i \mathbf{W}^q)(\mathbf{x}_j \mathbf{W}^k + \mathbf{r}_{i,j} \mathbf{W}^g)^\top}{\sqrt{b}} \right]_{i,j} \right), \quad (3)$$

$$\mathbf{z}_i = \sum_{j=1}^{|\hat{\mathbf{P}}|} a_{i,j} (\mathbf{x}_j \mathbf{W}^v) \quad (4)$$

where  $W^q, W^k, W^v, W^g \in \mathbf{R}_{b \times b}$  are linear projections of queries, keys, values and geometric structure embeddings. Given the self-attention feature  $Z^{\hat{\mathbf{P}}}$  and  $Z^{\hat{\mathbf{Q}}}$ , the cross-attention layer is define as:

$$a_{i,j} = \text{softmax} \left( \left[ \frac{(\mathbf{z}_i^{\hat{\mathbf{P}}})(\mathbf{z}_j^{\hat{\mathbf{Q}}})^\top}{\sqrt{b}} \right]_{i,j} \right), \quad (5)$$

$$\mathbf{z}_i^{\hat{\mathbf{P}}} = \sum_{j=1}^{|\hat{\mathbf{Q}}|} a_{i,j} (\mathbf{z}_j^{\hat{\mathbf{Q}}} \mathbf{W}^v). \quad (6)$$

where  $W^q, W^k, W^v \in \mathbf{R}_{b \times b}$  are linear projections of queries, keys, values.

By through three interleaved attention layers of the configuration 'self/cross/self', we get latent superpoint features  $\mathbf{F}^{\hat{\mathbf{P}}} \in \mathbf{R}^{N' \times b}$  and  $\mathbf{F}^{\hat{\mathbf{Q}}} \in \mathbf{R}^{M' \times b}$ . To avoid symbol abuse, the initial input and final output features of the attention layers are all noted as  $\mathbf{F}^{\hat{\mathbf{P}}} \in \mathbf{R}^{N' \times b}$  and  $\mathbf{F}^{\hat{\mathbf{Q}}} \in \mathbf{R}^{M' \times b}$ . From superpoint latent features, we can also compute *soft correspondence* of a super point  $\hat{p}_i$  (i.e., the probability that its matching point in  $\hat{\mathbf{Q}}$  lies in the overlap region):

$$\hat{o}_i^{\hat{\mathbf{P}}} = \mathbf{w}_i^\top \mathbf{o}^{\hat{\mathbf{Q}}}, \quad w_{ij} = \text{softmax} \left( \frac{1}{t} \langle \mathbf{f}_i^{\hat{\mathbf{P}}}, \mathbf{f}_j^{\hat{\mathbf{Q}}} \rangle \right) \quad (7)$$

To further optimize the latent feature, we add an Partial Graph Matching (PGM) constraint to enhance the super points' abilities to capture isometric preserving transformation properties. This constraint is decribed in section III-D.

3) *Point Feature Decoder:* Given the super point features, we need to recover the original resolution point features. We leverage the NN-upsampling and skip connections from encoder to form the decoder. We firstly concatenate the super point features  $F^{\hat{\mathbf{P}}}$ , overlap scores  $\tilde{O}^{\hat{\mathbf{P}}}$ , then go through upsampling decoder to get the fine level ones:  $\mathbf{F}^P \in \mathbf{R}^{N \times 32}$ ,  $\mathbf{O}^P$ , and  $\mathbf{M}^P$ . Finally, we add full graph matching constraint in fine level overlap region (see in section III-E).

#### D. Superpoint Partial Graph Matching Constraint

As mentioned in the introduction, we need to add task-specific prior knowledge that the isometry should be preserved after transformation.

Since our task is to make rigid registration on low overlap point cloud pairs, if we know the overlap ratio of two point cloud pair, we can solve the partial matching problem to obtain the matching matrix:

$$\begin{aligned} \min_{\Gamma \in \Pi(\mathbf{p}, \mathbf{q})} \sum_{i=1}^N \sum_{j=1}^M \mathbf{C}_{ij}^{\hat{\mathbf{P}}\hat{\mathbf{Q}}} \Gamma_{ij} + \frac{1}{2} \sum_{i,k=1}^N \sum_{j,l=1}^M \left( \mathbf{C}_{ik}^{\hat{\mathbf{P}}} - \mathbf{C}_{jl}^{\hat{\mathbf{Q}}} \right)^2 \Gamma_{ij} \Gamma_{kl} \\ = \min_{\Gamma \in \Pi(\mathbf{p}, \mathbf{q})} \langle \mathbf{C}^{\hat{\mathbf{P}}\hat{\mathbf{Q}}}, \Gamma \rangle + \langle \mathbf{L}(\mathbf{C}^{\hat{\mathbf{P}}}, \mathbf{C}^{\hat{\mathbf{Q}}}, \Gamma), \Gamma \rangle, \end{aligned} \quad (8)$$

where  $\langle \cdot \rangle$  is inner product,  $\mathbf{L}(\mathbf{C}^{\hat{\mathbf{P}}}, \mathbf{C}^{\hat{\mathbf{Q}}}, \Gamma) = [\mathbf{L}_{jj'}] \in \mathbf{R}^{N \times M}$ , each  $\mathbf{L}_{jj'} = \sum_{i,i'} \mathcal{L}(\mathbf{C}_{ij}^{\hat{\mathbf{P}}}, \mathbf{C}_{i'j'}^{\hat{\mathbf{Q}}}) \Gamma_{ii'}$ , and  $\mathcal{L}(a, b) = \frac{1}{2}(a-b)^2$ . The admissible couplings  $\Pi(\mathbf{p}, \mathbf{q})$  are defined as  $\{\Gamma \in \mathbf{R}_+^{N \times M} | \Gamma \mathbf{1}_N \leq \mathbf{1}_M, \Gamma^\top \mathbf{1}_M \leq \mathbf{1}_N, \mathbf{1}_N^\top \Gamma \mathbf{1}_M = s\}$ . The affinity matrices  $\mathbf{C}^{\hat{\mathbf{P}}}$ ,  $\mathbf{C}^{\hat{\mathbf{Q}}}$ , and  $\mathbf{C}^{\hat{\mathbf{P}}\hat{\mathbf{Q}}}$  are computed from super points' coordinates and features:

$$\begin{aligned} [\mathbf{C}^{\hat{\mathbf{P}}}]_{ij} &= \|\mathbf{f}_i^{\hat{\mathbf{P}}} - \mathbf{f}_j^{\hat{\mathbf{P}}}\|_2 + o^{\hat{p}_i} o^{\hat{p}_j} \alpha \|\hat{\mathbf{p}}_i - \hat{\mathbf{p}}_j\|_2, \\ [\mathbf{C}^{\hat{\mathbf{Q}}}]_{ij} &= \|\mathbf{f}_i^{\hat{\mathbf{Q}}} - \mathbf{f}_j^{\hat{\mathbf{Q}}}\|_2 + o^{\hat{q}_i} o^{\hat{q}_j} \alpha \|\hat{\mathbf{q}}_i - \hat{\mathbf{q}}_j\|_2, \\ [\mathbf{C}^{\hat{\mathbf{P}}\hat{\mathbf{Q}}}]_{ij} &= \|\mathbf{f}_i^{\hat{\mathbf{P}}} - \mathbf{f}_j^{\hat{\mathbf{Q}}}\|_2, \end{aligned} \quad (9)$$

where  $o^{\hat{p}_i}$  and  $o^{\hat{q}_j}$  are overlap region scores of super points  $\hat{\mathbf{p}}_i$  and  $\hat{\mathbf{q}}_j$ , and  $\alpha$  is hyper-parameter. To focus on the overlap region, we add the overlap score to the second part of  $[\mathbf{C}^{\hat{\mathbf{P}}}]_{ij}$  and  $[\mathbf{C}^{\hat{\mathbf{Q}}}]_{ij}$ . The empirical distributions  $(\mathbf{p}, \mathbf{q}) \in \Sigma_N \times \Sigma_M$ ,  $\Sigma_N$  is a histogram of  $N$  bins with  $\{\mathbf{p} \in \mathbf{R}_+^N, \sum_i p_i = 1\}$ .  $\mathbf{o}^{\hat{\mathbf{P}}}$  and  $\mathbf{o}^{\hat{\mathbf{Q}}}$  are overlap scores. In line 1 of the Algorithm10, we utilize the uniform distribution to initialize  $(\mathbf{p}, \mathbf{q})$ . The partial transport mass  $s$  is computed from the super points' anchored patch [14] pairs whose overlap ratio is higher than 10%.

Since the proximal point method is an efficient algorithm to solve the non-convex problem, motivated by [29], in the  $n$ -th iteration, we update correspondence matrix  $\Gamma$  as:

$$\Gamma^{n+1} = \arg \min_{\Gamma \in \Pi(\mathbf{p}, \mathbf{q})} \langle \mathbf{C}^{\hat{\mathbf{P}}\hat{\mathbf{Q}}}, \Gamma \rangle + \langle \mathbf{L}(\mathbf{C}^{\hat{\mathbf{P}}}, \mathbf{C}^{\hat{\mathbf{Q}}}, \Gamma), \Gamma \rangle + \varepsilon KL(\Gamma | \Gamma^n), \quad (10)$$

where  $KL(a||b) = a \log(\frac{a}{b}) - a + b$ .

Inspired by [26], by using mirror descent and Bregman projection (i.e., both the gradient and the projection are computed in the  $KL$  metric) and setting the learning rate to  $\frac{1}{\varepsilon}$ , we can transform problem (10) to a new  $\varepsilon$ -convex entropic regularized optimal transport problem:

$$\Gamma^{n+1} = \arg \min_{\Gamma \in \Pi(\mathbf{p}, \mathbf{q})} \langle \bar{\mathbf{C}}^n - \varepsilon \log \Gamma^n, \Gamma \rangle + \varepsilon H(\Gamma), \quad (11)$$

where  $\bar{\mathbf{C}}^n = L(\mathbf{C}^{\hat{\mathbf{P}}}, \mathbf{C}^{\hat{\mathbf{Q}}}, \Gamma^n) + \mathbf{C}^{\hat{\mathbf{P}}\hat{\mathbf{Q}}}$  and the entropy  $H(\Gamma) = -\sum_{i,j=1}^N \Gamma_{i,j} (\log(\Gamma_{i,j}) - 1)$ . According to Proposition 5 in [60], problem (11) is a partial transport problem with inequality constraints, which needs to use the Dykstra's algorithm [61] to solve it, see Algorithm 1.

To accelerate the computing speed, motivated by the inexact proximal point algorithm (IPOT) in [29], the inner number of Dykstra's iterations  $L$  is set to 1, as shown in Algorithm 1.

#### E. Mini-batch Full Graph Matching in Overlap Region

In order to further optimize the point-matching score in the global scope for the fine-level points in the overlapping regions, we propose the relaxed Graph Matching Optimization method (Koopmans-Beckmann's QAP) to add the second-order constraint:

$$\min_{\Gamma \in \Pi(\mathbf{p}, \mathbf{q})} \mathbf{J}_{gm}(\Gamma) = \min_{\Gamma} \|\mathbf{C}^P - \Gamma \mathbf{C}^Q \Gamma^\top\|_F + Tr(\mathbf{C}^{PQ^\top} \Gamma), \quad (12)$$

where  $\mathbf{C}^P$  and  $\mathbf{C}^Q$  are two affinity matrices of two graphs generated from point clouds  $\mathbf{P}$  and  $\mathbf{Q}$ , respectively.  $\mathbf{C}^{PQ}$  is the inter-graph affinity matrix or cost matrix.  $\hat{\Pi}(\mathbf{p}, \mathbf{q})$  is

---

**Algorithm 1:** Inexact Proximal Optimal Transport for Partial Graph Matching (IPOT-PGM)

---

**Input:** Intra-affinity matrix  $\mathbf{C}^P$  and  $\mathbf{C}^Q$ , Inter-affinity matrix  $\mathbf{C}^{\hat{P}\hat{Q}}$ , Overlap ratio  $s$ , Probabilities  $\{\mathbf{p}, \mathbf{q}\}$  on support points  $\{\hat{\mathbf{P}}, \hat{\mathbf{Q}}\}$ , Entropy regularized weight  $\varepsilon$ .

**Output:** Correspondence matrix  $\Gamma^K$

- 1 Initialize  $\Gamma^0 = \mathbf{p}\mathbf{q}^\top$
- 2 **for**  $n = 0 : K - 1$  **do**
  - /\* Efficiently computing  $\tilde{\mathbf{C}}^n$  in Eqn. (11), see Proposition 1 in [26].
  - $f_1(a) = a^2, f_2(b) = b^2, h_1(a) = a, h_2(b) = 2b$  \*/
  - 3  $\text{Cost}^{\hat{P}\hat{Q}} = f_1(\mathbf{C}^{\hat{P}})\mathbf{p}\mathbf{1}_M^\top + \mathbf{1}_N\mathbf{q}^\top f_2(\mathbf{C}^{\hat{Q}})^\top$
  - 4  $\tilde{\mathbf{C}}^n = \text{Cost}^{\hat{P}\hat{Q}} - h_1(\mathbf{C}^P)\Gamma^n h_2(\mathbf{C}^Q)^\top + \mathbf{C}^{\hat{P}\hat{Q}}$
  - 5 Set  $\mathbf{G} = \exp\left(\frac{-\tilde{\mathbf{C}}^n}{\varepsilon}\right) \odot \Gamma^n$   
// Usually set  $L=1$  for Inexact Proximal
  - 6 **for**  $l = 1, 2, 3 \dots L$  **do**
    - /\* Dykstra's iterations
    - 7  $\mathbf{G} = \text{diag}\left(\min\left(\frac{\mathbf{p}}{\mathbf{1}_M}, \mathbf{1}_N\right)\right)\mathbf{G}$
    - 8  $\mathbf{G} = \mathbf{G}\text{diag}\left(\min\left(\frac{\mathbf{q}}{\mathbf{1}_N}, \mathbf{1}_M\right)\right)$
    - 9  $\mathbf{G} = \mathbf{G} \odot \frac{s}{\mathbf{1}_N\mathbf{1}_M}$
- 10  $\Gamma^K = \mathbf{G}$

---

defined as  $\{\Gamma \in \mathbb{R}_+^{N \times M} | \Gamma \geq 0, \Gamma \mathbf{1}_N \leq \mathbf{1}_M, \Gamma^\top \mathbf{1}_M \leq \mathbf{1}_N\}$ . The definitions of  $\mathbf{C}^P$ ,  $\mathbf{C}^Q$ , and  $\mathbf{C}^{\hat{P}\hat{Q}}$  are as follows:

$$\begin{aligned} [\mathbf{C}^P]_{ij} &= \|\mathbf{f}_i^P - \mathbf{f}_j^P\|_2 + \alpha \|\mathbf{p}_i - \mathbf{p}_j\|_2, \\ [\mathbf{C}^Q]_{ij} &= \|\mathbf{f}_i^Q - \mathbf{f}_j^Q\|_2 + \alpha \|\mathbf{q}_i - \mathbf{q}_j\|_2, \\ [\mathbf{C}^{\hat{P}\hat{Q}}]_{ij} &= \|\mathbf{f}_i^P - \mathbf{f}_j^Q\|_2, \end{aligned} \quad (13)$$

where  $\alpha$  is a hyper-parameter that controls the geometric similarity. The optimizing object in this problem is non-convex since the existence of the quadratic term (i.e., the first part of object in (12)). A typical way to solve this problem is to add  $M - N$  dummy nodes to point cloud  $\mathbf{P}$  to make a square matching matrix  $\Gamma$ . Then a path-following strategy [56] can be adopted to make gradually non-convex optimization to solve this problem, and Frank-Wolfe's algorithm [55] is used in this strategy. For the big graph matching problem (e.g.,  $M > 100$ ), Factorized Graph Matching (FGM) [24] may be an available tool. However, the matching matrix needs to be full rank (i.e., overlap ratio is 100%) in the concave-convex relaxation, so we use it to optimize the full graph matching of correspondences in the overlap region. Furthermore, since Koopmans-Beckmann's QAP can be represented as a particular case of Lawler's QAP, we utilize a reduced path following algorithm to solve the problem (12), as shown in Algorithm 2. Since the scale of point cloud data is large, it is hard to directly use optimal transport on large-scale point cloud problems. The typical application of optimal transport is to use it to refine the coarse matching matrix [13].

Recently, a straightforward and scalable way [30], [58] is proposed that computes OT correspondences over subsets

---

**Algorithm 2:** The Path Following Method for mini-batch Graph Matching (mbGM).

---

**Input:** Points and features of sampled mini-batch  $\mathbf{p}_i^m, \mathbf{q}_i^m$  in overlap region.

**Output:** Permutation matrix in overlap region  $\Gamma_{\alpha=1, k=K}$ .

- 1 Initialize  $\mathbf{C}^{P^m}, \mathbf{C}^{Q^m}$ , and  $\mathbf{C}^{P^m Q^m}$  from points and features of  $\mathbf{p}_i^m, \mathbf{q}_i^m$ .
- 2 Initialize  $\Gamma_0$  from features of sampled mini-batch  $\mathbf{p}_i^m, \mathbf{q}_i^m$ .
- 3 /\* Const item. \*/
- 4  $\mathbf{J}_{\text{con}}(\Gamma) = \text{Tr}(\mathbf{C}^{P^m \top} \Gamma \Gamma^\top \mathbf{C}^{P^m}) + \text{Tr}(\mathbf{C}^{Q^m} \Gamma^\top \Gamma \mathbf{C}^{Q^m \top})$   
/\* Convex part. \*/
- 5  $\mathbf{J}_{\text{vex}}(\Gamma) = \mathbf{J}_{\text{gm}}(\Gamma) - \frac{1}{2} \mathbf{J}_{\text{con}}(\Gamma)$   
/\* Concave part. \*/
- 6  $\mathbf{J}_{\text{cav}}(\Gamma) = \mathbf{J}_{\text{gm}}(\Gamma) + \frac{1}{2} \mathbf{J}_{\text{con}}(\Gamma)$   
/\* Convex-concave relaxation of  $\mathbf{J}_{\text{gm}}(\Gamma)$ . \*/
- 7  $\mathbf{J}_\alpha(\Gamma) = (1 - \alpha) \mathbf{J}_{\text{vex}}(\Gamma) + \alpha \mathbf{J}_{\text{cav}}(\Gamma)$   
/\* Computation of gradient of  $\mathbf{J}_\alpha(\Gamma)$ , and we set  $\text{Rank}(\mathbf{C}^{P^m Q^m})=1$  for acceleration. \*/
- 8  $P_u = \mathbf{C}^{P^m} - \Gamma \mathbf{C}^{Q^m} \Gamma^\top, P_v = \mathbf{C}^{P^m} + \Gamma \mathbf{C}^{Q^m} \Gamma^\top$
- 9  $\nabla \mathbf{J}_{\text{vex}}(\Gamma) = -P_u^\top \Gamma \mathbf{C}^{Q^m} - P_u \Gamma \mathbf{C}^{Q^m \top} - \mathbf{C}^{P^m Q^m}$
- 10  $\nabla \mathbf{J}_{\text{cav}}(\Gamma) = P_v^\top \Gamma \mathbf{C}^{Q^m} + P_v \Gamma \mathbf{C}^{Q^m \top} - \mathbf{C}^{P^m Q^m}$
- 11  $\nabla \mathbf{J}_\alpha(\Gamma) = (1 - \alpha) \nabla \mathbf{J}_{\text{vex}}(\Gamma) + \alpha \nabla \mathbf{J}_{\text{cav}}(\Gamma)$   
/\* A reduced Path following algorithm.  $\delta$  is usually set to 0.1. *Sinkhorn<sub>proj</sub>* is Sinkhorn normalization [38]. \*/
- 12 **for**  $\alpha := 0 : \delta : 1$  **do**
- 13 **for**  $k := 1 : K - 1$  **do**
- 14  $y_k = \text{argmin}_y \nabla \mathbf{J}_\alpha(\Gamma_k)^\top y$
- 15  $s = \text{Sinkhorn}_{\text{proj}}(y_k)$
- 16  $\varepsilon_k = \frac{2}{k+2}$
- 17  $\tilde{\Gamma}_{k+1} = \tilde{\Gamma}_k - \varepsilon_k (\tilde{\Gamma}_k - s)$
- 18  $\Gamma_{k+1} = \text{Sinkhorn}_{\text{proj}}(\tilde{\Gamma}_{k+1})$

---

(mini-batch) of the original data and averages the resulting matching matrix as an approximation of the original solution. Despite the limits of this strategy, researchers utilize the unbalanced optimal transport [62] or partial optimal transport [61] to improve it. Therefore, we take the mini-batch optimal transport (m-OT) to solve the graph matching problem in the overlap region:

*Definition 1:* (Mini-batch Graph Matching) For subset size  $1 \leq m \leq \min(M, N)$  and subsets number  $K \geq 1$ ,  $\mathbf{p}_1^m, \dots, \mathbf{p}_K^m$  and  $\mathbf{q}_1^m, \dots, \mathbf{q}_K^m$  are subsets that are sampled from the overlap region of point clouds  $\mathbf{P}$  and  $\mathbf{Q}$ , respectively. The mini-batch transport plan is:

$$\begin{aligned} \Gamma^{m, K, s} &= \frac{1}{K} \sum_{i=1}^K \Gamma(\mathbf{p}_i^m, \mathbf{q}_i^m), \\ \Gamma(\mathbf{p}_i^m, \mathbf{q}_i^m) &= \arg \min_{\Gamma \in \Pi(\mathbf{p}_i^m, \mathbf{q}_i^m)} \|\mathbf{C}^{P^m} - \Gamma \mathbf{C}^{Q^m} \Gamma^\top\|_F + \text{Tr}(\mathbf{C}^{P^m Q^m \top} \Gamma), \end{aligned} \quad (14)$$

where  $(\mathbf{p}_i^m, \mathbf{q}_i^m)$  are two empirical distributions computed from two subsets  $\mathbf{p}_i^m$  and  $\mathbf{q}_i^m$ .

We uniformly sample  $K$  subsets from the fine-level overlap region, and each subset contains  $m$  points. The average of  $K$  mini-batch solutions would give an approximation of ground truth correspondences.

## F. Loss Function

**Coarse-level Overlap-aware Circle loss:** Inspired by [14], the overlap ratio of patches anchored on the super points can weight the positive matching in loss to avoid the issue that the circle loss weights the positive samples equally. Given a pair of aligned coarse-level super points  $\hat{\mathbf{P}}$  and  $\hat{\mathbf{Q}}$ . A pair of super points is positive if their anchor patch shares at least a 10% overlap ratio and negative if there is no overlap. All other pairs are dropped. For a super point  $\hat{p}_i$ , which at least has one positive patch in  $\hat{\mathbf{Q}}$ , we define the super points in  $\hat{\mathbf{Q}}$  within radius  $r_{\hat{p}}$  as  $\xi_p(\hat{p}_i)$  and the super points outside a larger radius  $r_n$  as  $\xi_n(\hat{p}_i)$ . Inspired by [13], [14], we sampled  $n_p$  points from  $\hat{p}_i$ , and the circle loss can be defined as follows:

$$\mathcal{L}_{coc}^{\hat{\mathbf{P}}} = \frac{1}{n_p} \sum_{i=1}^{n_p} \log \left[ 1 + \sum_{j \in \xi_p(\hat{p}_i)} e^{\lambda_i^j \gamma (d_i^j - \Delta_p)} + \sum_{k \in \xi_n(\hat{p}_i)} e^{\gamma (\Delta_n - d_i^k)} \right], \quad (15)$$

where  $d_i^j = \|\mathbf{f}^{\hat{p}_i} - \mathbf{f}^{\hat{q}_j}\|_2$ ,  $\gamma$  is a hyper-parameters and  $\lambda_i^j$  is the overlap ratio of patches anchored on super point  $\hat{p}_i$  and  $\hat{q}_j$ . Two empirical margins are defined as  $\Delta_p := 0.1$  and  $\Delta_n := 1.4$ . The reverse loss  $\mathcal{L}_{coc}^{\hat{\mathbf{Q}}}$  is also defined in the same way and the final circle loss is  $\mathcal{L}_{coc} = \frac{1}{2}(\mathcal{L}_{coc}^{\hat{\mathbf{P}}} + \mathcal{L}_{coc}^{\hat{\mathbf{Q}}})$ .

**Coarse-level Partial Graph Matching loss:** Based on the coarse-level super points and features, we calculate the intra-affinity and inter-affinity matrix for Eqn.(11). The solution of partial graph matching optimization problem (i.e., Eqn.(11)) can be treated as overlap scores. The supervision on the overlap score can be cast a binary classification, and we define a cross-entropy loss:

$$\mathcal{L}_{cpgm}^{\hat{\mathbf{P}}} = \frac{1}{|\hat{\mathbf{P}}|} \sum_{i=1}^{\hat{\mathbf{P}}} \bar{o}^{\hat{p}_i} \log(o^{\hat{p}_i}) + (1 - \bar{o}^{\hat{p}_i}) \log(1 - o^{\hat{p}_i}), \quad (16)$$

where ground truth  $\bar{o}^{\hat{p}_i}$  is based on the overlap ratio of patch pairs that  $\bar{o}^{\hat{p}_i}$  is 1 if the overlap ratio is greater than 10%, otherwise 0. The reverse loss  $\mathcal{L}_{cpgm}^{\hat{\mathbf{Q}}}$  is also defined in the same way, and the final loss is  $\mathcal{L}_{cpgm} = \frac{1}{2}(\mathcal{L}_{cpgm}^{\hat{\mathbf{P}}} + \mathcal{L}_{cpgm}^{\hat{\mathbf{Q}}})$ .

### Fine-Level mini-batch Graph Matching loss:

The loss supervising the predicted correspondences in the overlap region is defined as:

$$\mathcal{L}_{mbm}^{\mathbf{P}} = \frac{1}{|\mathbf{P}|} \sum_{i=1}^{\mathbf{P}} \bar{m}^{p_i} \log(m^{p_i}) + (1 - \bar{m}^{p_i}) \log(1 - m^{p_i}), \quad (17)$$

where  $\bar{m}^{p_i}$  is ground truth and  $m^{p_i}$  is solution of problem (12). The reverse loss  $\mathcal{L}_{mbm}^{\mathbf{Q}}$  is also defined in the same way and final circle loss is  $\mathcal{L}_{mbm} = \frac{1}{2}(\mathcal{L}_{mbm}^{\mathbf{P}} + \mathcal{L}_{mbm}^{\mathbf{Q}})$ .

**Other three fine-level losses:** Inspired by [12], we add two losses to supervise the overlap probability, and the matchability scores on the fine level points and one circle loss to learn the point-wise feature. We use a binary classification loss to supervise the overlap probability:

$$\mathcal{L}_o^{\mathbf{P}} = \frac{1}{|\mathbf{P}|} \sum_{i=1}^{\mathbf{P}} \bar{o}^{p_i} \log(o^{p_i}) + (1 - \bar{o}^{p_i}) \log(1 - o^{p_i}), \quad (18)$$

where ground truth label  $\bar{o}^{p_i}$  is defined as

$$\bar{o}^{p_i} = \begin{cases} 1, & \|\mathbf{T}(\mathbf{p}_i) - \mathbf{NN}(\mathbf{T}(\mathbf{p}_i), \mathbf{Q})\|_2 < \varepsilon_o \\ 0, & \text{otherwise} \end{cases}, \quad (19)$$

with overlap threshold  $\varepsilon_o$ . The reverse loss  $\mathcal{L}_o^{\mathbf{Q}}$  is computed in the same way and  $\mathcal{L}_o = \frac{1}{2}(\mathcal{L}_o^{\mathbf{P}} + \mathcal{L}_o^{\mathbf{Q}})$ . Similarly, we also use a binary classification loss to supervise the matching score:

$$\mathcal{L}_m^{\mathbf{P}} = \frac{1}{|\mathbf{P}|} \sum_{i=1}^{\mathbf{P}} \hat{m}^{p_i} \log(m^{p_i}) + (1 - \hat{m}^{p_i}) \log(1 - m^{p_i}), \quad (20)$$

where ground truth labels  $\hat{m}^{p_i}$  are generated on the fly

$$\hat{m}^{p_i} = \begin{cases} 1, & \|\mathbf{T}(\mathbf{p}_i) - \mathbf{NN}_F(\mathbf{T}(\mathbf{p}_i), \mathbf{Q})\|_2 < \varepsilon_m \\ 0, & \text{otherwise} \end{cases}, \quad (21)$$

via nearest neighbour search  $\mathbf{NN}_F(\cdot, \cdot)$  in feature space with overlap threshold  $\varepsilon_m$ . The reverse loss  $\mathcal{L}_m^{\mathbf{Q}}$  is defined in the same way and  $\mathcal{L}_m = \frac{1}{2}(\mathcal{L}_m^{\mathbf{P}} + \mathcal{L}_m^{\mathbf{Q}})$ . The circle loss  $\mathcal{L}_c$  defined on fine level points  $\mathbf{P}$  and  $\mathbf{Q}$  is similar to  $\mathcal{L}_{coc}$  except without the overlap ratio coefficient  $\lambda_i^j$ . The final loss is defined as

$$\mathcal{L} = \lambda_c(\mathcal{L}_{coc} + \mathcal{L}_{cpgm}) + \lambda_f(\mathcal{L}_{mbm} + \mathcal{L}_c + \mathcal{L}_o + \mathcal{L}_m), \quad (22)$$

where  $\lambda_c$  and  $\lambda_f$  are the weights of the coarse-level and the fine-level losses, respectively. Following [13], we set  $\lambda_c = \lambda_f = 1$ .

## IV. EXPERIMENTS

### A. Experimental Settings

Following [12], we evaluate the proposed GMONet on indoor datasets 3DMatch [34] and 3DLoMatch [12] and outdoor KITTI odometry [63] benchmark.

**Implementation and training:** The proposed GMONet is implemented and tested with PyTorch [64] on Xeon(R) Gold 6230 and one NVIDIA RTX TITAN GPU. The network is trained 30 epochs on the 3DMatch/3DLoMatch dataset and 150 epochs on the KITTI odometry benchmark, all with Adam optimizer. The learning rates for 3DMatch/3DLoMatch and KITTI are set to 1e-4 and 5e-2, respectively. The batch size, weight decay, and momentum are set as 1, 1e-6, and 0.98, respectively. 3DMatch and KITTI's matching radii are set to 5cm and 30cm, respectively. The hyper-parameter  $\alpha$  in III-D is set to 0.01. The other parameters are the same as [12].

### B. Indoor dataset: 3DMatch and 3DLoMatch

**Dataset.** 3DMatch [34] contains 62 scenes, divided into 46, 8, and 8 for training, validating, and testing, respectively. The overlap ratio of scanned pairs in 3DMatch are greater than 30%, while 10%-30% in 3DLoMatch.

**Metrics.** Following [34], we report performance with three metrics: (1) rigid Registration Recall (RR), the fraction of point cloud pairs whose correspondence RMSE below 0.2m. (2) Relative Rotation Error (RRE), the geodesic distance between estimated and ground truth rotation matrices. (3) Relative Translation Error (RTE), the Euclidean distance

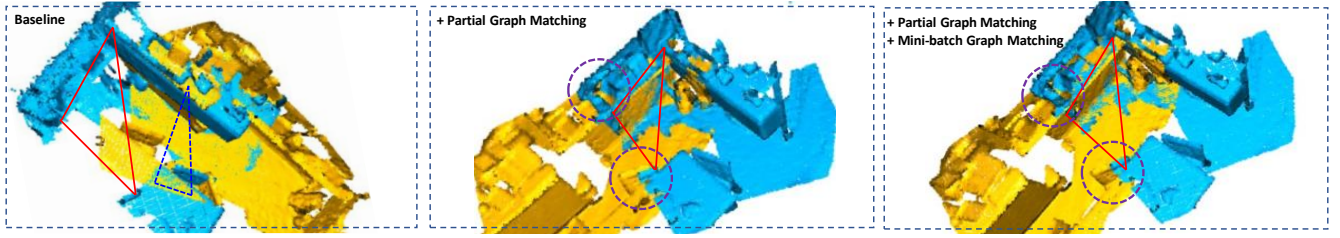


Fig. 2. Visualization of the effective role of coarse-level partial graph matching constraint and fine-level graph matching constraint.

between the estimated and ground truth translation. RRE and RTE are calculated on the successfully matching scan pairs.

Since the high inlier ratio does not necessarily lead to high registration recall as the correspondences could cluster together as noted in [12], we skip other two metrics Feature Matching Recall (FMR) and Inlier Ratio (IR) in the benchmark comparison. The RTE and RRE are defined as mean error of successfully registered ones.

**Interest point sampling.** Our interest point sampling strategy is the same as [12]. In the evaluation stage, we multiply the overlapping scores and global matching scores as the inlier confidence probabilities of points. Then a random sampling based on the confidence probability is applied to obtain the candidate point correspondences.

**Results.** We compare GMONet to recent **feature-matching-based** methods (FCGF [10], D3Feat [9], Predator [12], CoFiNet [13], GeoTransformer [14]). For fairly comparison, we adopt the same sampling strategy as GMONet for evaluation of baseline GeoTransformer [14].

Tab.I shows that GMONet achieves the best registration recall to 92.1% on 3DMatch and 73.2% on 3DLoMatch with a sampling of 1000 points. Our method achieves relatively lower RTE and RRE on both 3DMatch and 3DLoMatch benchmarks. This reveals that, by adding two graph matching constraints in learning stage, the point features indeed learns the isometry preserving features and help to select more precisely the good candidate corresponding point.

**Ablation studies.** In the ablation studies, we take KPConv [11] as the backbone plus geometric attention layer, coarse-level overlap-aware circle loss, and three fine-level losses as baseline. Then we add two levels of graph matching loss to conduct extensive experiments to ablate how these two constraints improve the feature representation of the baseline. The number of sampling points is set to 1000. Tab.II illustrates that by adding partial graph matching constraint on the coarse-level super points, the registration recall increases 0.58 percent points (pp) on 3DMatch and 0.6 pp on 3DLoMatch. The mini-batch graph matching constraint on fine-level points improves by 1.38 pp on 3DMatch and 3.0 pp on 3DLoMatch, respectively. These two constraints combined improve 2.08 pp and 5.0 pp on 3DMatch and 3DLoMatch, respectively.

As visualized in Fig.2, without explicit second-order constraints, RANSAC estimation would prefer such correspondences, *e.g.*, edges of the **deep blue triangle**, that meet the

TABLE I  
QUANTITATIVE RESULTS ON THE 3DMatch AND 3DLoMatch BENCHMARKS. BEST RESULTS ARE HIGHLIGHTED IN BOLD, AND SECOND BEST RESULTS ARE UNDERLINED.

# Samples	3DMatch					3DLoMatch				
	5000	2500	1000	500	250	5000	2500	1000	500	250
RR (%)↑										
FCGF [10]	85.1	84.7	83.3	81.6	71.4	40.1	41.7	38.2	35.4	26.8
D3Feat [9]	81.6	84.5	83.4	82.4	77.9	37.2	42.7	46.9	43.8	39.1
Predator [12]	89.0	89.9	90.6	88.5	86.6	59.8	61.2	62.4	60.8	58.1
CoFiNet [13]	89.3	88.9	88.4	87.4	87.0	67.5	66.2	64.2	63.1	61.0
GeoTransformer [14]	<b>91.4</b>	<u>91.3</u>	<u>91.4</u>	<u>90.8</u>	<b>90.4</b>	<b>72.3</b>	<u>72.0</u>	<u>71.7</u>	<u>72.3</u>	<b>71.3</b>
GMONet	91.3	<b>91.8</b>	<b>92.1</b>	<b>91.0</b>	<u>89.5</u>	69.0	<b>72.4</b>	<b>73.2</b>	<b>72.6</b>	69.9
RTE (m)↓										
FCGF [10]	0.066	-	<u>0.066</u>	-	-	-	-	0.105	-	-
D3Feat [9]	0.067	-	-	-	-	-	-	-	-	-
Predator [12]	<u>0.064</u>	<u>0.063</u>	<u>0.068</u>	<b>0.069</b>	0.076	0.091	<u>0.089</u>	<u>0.092</u>	0.102	0.108
CoFiNet [13]	<u>0.064</u>	<u>0.063</u>	0.069	0.070	0.074	0.090	0.095	0.096	0.099	0.107
GeoTransformer [14]	0.070	0.069	0.071	<u>0.070</u>	<b>0.072</b>	0.097	0.099	0.099	0.101	<b>0.101</b>
GMONet	<b>0.061</b>	<b>0.062</b>	<b>0.063</b>	0.071	0.077	<b>0.089</b>	<b>0.089</b>	<b>0.088</b>	<b>0.093</b>	0.109
RRE (°)↓										
FCGF [10]	1.949	-	<u>2.060</u>	-	-	-	-	3.820	-	-
D3Feat [9]	2.161	-	-	-	-	-	-	-	-	-
Predator [12]	1.847	1.869	1.998	2.169	<b>2.468</b>	3.156	3.124	3.368	3.675	3.927
CoFiNet [13]	2.002	2.124	2.281	2.302	2.486	3.271	3.415	3.520	3.513	3.748
GeoTransformer [14]	2.021	2.041	2.072	<b>2.019</b>	2.134	3.238	3.383	<u>3.267</u>	<b>3.298</b>	<b>3.472</b>
GMONet	<b>1.841</b>	<b>1.857</b>	<b>1.857</b>	<u>2.059</u>	<u>2.500</u>	<b>2.856</b>	<b>2.959</b>	<b>2.937</b>	<u>3.300</u>	<u>3.637</u>

TABLE II  
ABLATION OF THE NETWORK ARCHITECTURE ON 3DMatch/3DLoMatch BENCHMARK. TESTED WITH SAMPLES=1000.

		3DMatch			3DLoMatch		
mbGM	IPOT-PGMP	RR (%)	RRE (°)	RTE (cm)	RR (%)	RRE (°)	RTE (cm)
		90.02	2.014	0.065	68.2	3.070	0.092
		91.40	1.875	0.063	71.2	2.860	0.090
✓		90.60	1.946	0.063	68.8	3.062	0.089
✓	✓	92.10	1.857	0.063	73.2	2.937	0.088

TABLE III  
QUANTITATIVE RESULTS ON THE KITTI ODOMETRY BENCHMARK. BEST RESULTS ARE HIGHLIGHTED IN BOLD, AND SECOND BEST RESULTS ARE UNDERLINED.

Method	RTE (cm)↓	RRE (°)↓	RR (%)↑
3DFeat-Net	25.9	<b>0.25</b>	96.0
FCGF [10]	9.5	0.30	<u>96.6</u>
D3Feat [9]	7.2	0.30	<u>99.8</u>
Predator [12]	<b>6.8</b>	0.27	<b>99.8</b>
CoFiNet [13]	8.2	0.41	<b>99.8</b>
GeoTransformer [14]	7.4	0.27	<b>99.8</b>
GMONet	<b>6.8</b>	<u>0.27</u>	<b>99.8</b>

hypothesis of max consensus (pseudo) inlier correspondences (see the left failure case). However, by explicitly adding two isometric preserving constraints, the point feature would recognize sparse correspondences (e.g., edges of the red triangle) even though the candidate corresponding points are far from each other in the euclidean space. Moreover, the graph matching constraint on fine-level points further improves the registration’s precision (see points in the purple circle). This illustrates that the two levels of graph matching constraints indeed help to strengthening the isometry preserving in feature space.

### C. Outdoor dataset: KITTI Odometry

**Dataset.** KITTI Odometry benchmark [63] consists of 11 sequences of point clouds scanned by LiDAR. We follow [12], [14] to use sequences 0-5 for training, 6-7 for validation, and 8-10 for testing.

**Metrics.** Following [12], we evaluate GMONet with three metrics: (1) rigid Registration Recall (RR), the fraction of successful registration pairs (i.e.,  $RRE < 5^\circ$  and  $RTE < 2m$ ). The definitions of Relative Rotation Error (RRE) and Relative Translation Error (RTE) are the same as used in the 3DMatch benchmark.

**Results.** In the Tab.III, we compared GMONet with several state-of-the-art RANSAC-based methods: 3DFeat-Net [65], FCGF [10], D3Feat [9], Predator [12], CoFiNet [13], and GeoTransformer [14]. The quantitative results show that our method can handle outdoor scene registration and achieve competitive performance.

## V. CONCLUSION

We proposed a novel framework that integrates rigid isometry preserving constraints in the point feature learning stage. Specifically, we used the partial graph matching constraint at the coarse level and mini-batch full graph matching constraint at the fine level. Experimental results show that our method has competitive performance for point cloud registration task. In the future, we would like to verify our method on 2D-2D and 2D-3D tasks.

## REFERENCES

- [1] J. L. Schonberger and J.-M. Frahm, “Structure-from-motion revisited,” in *Proceedings of the IEEE conference on computer vision and pattern recognition*, 2016, pp. 4104–4113.
- [2] S. Choi, Q.-Y. Zhou, and V. Koltun, “Robust reconstruction of indoor scenes,” in *Proceedings of the IEEE Conference on Computer Vision and Pattern Recognition*, 2015, pp. 5556–5565.
- [3] J. Zhang and S. Singh, “Visual-lidar odometry and mapping: Low-drift, robust, and fast,” in *2015 IEEE International Conference on Robotics and Automation (ICRA)*. IEEE, 2015, pp. 2174–2181.
- [4] B. Drost, M. Ulrich, N. Navab, and S. Ilic, “Model globally, match locally: Efficient and robust 3d object recognition,” in *2010 IEEE computer society conference on computer vision and pattern recognition*. Ieee, 2010, pp. 998–1005.
- [5] A. Zeng, K.-T. Yu, S. Song, D. Suo, E. Walker, A. Rodriguez, and J. Xiao, “Multi-view self-supervised deep learning for 6d pose estimation in the amazon picking challenge,” in *2017 IEEE international conference on robotics and automation (ICRA)*. IEEE, 2017, pp. 1386–1383.
- [6] H. Yang, J. Shi, and L. Carlone, “Teaser: Fast and certifiable point cloud registration,” *IEEE Transactions on Robotics*, vol. 37, no. 2, pp. 314–333, 2020.
- [7] Q. Li, S. Chen, C. Wang, X. Li, C. Wen, M. Cheng, and J. Li, “Lo-net: Deep real-time lidar odometry,” in *Proceedings of the IEEE/CVF Conference on Computer Vision and Pattern Recognition*, 2019, pp. 8473–8482.
- [8] J. Zhang and S. Singh, “Loam: Lidar odometry and mapping in real-time,” in *Robotics: Science and Systems*, vol. 2, no. 9. Berkeley, CA, 2014, pp. 1–9.
- [9] X. Bai, Z. Luo, L. Zhou, H. Fu, L. Quan, and C.-L. Tai, “D3feat: Joint learning of dense detection and description of 3d local features,” in *Proceedings of the IEEE/CVF conference on computer vision and pattern recognition*, 2020, pp. 6359–6367.
- [10] C. Choy, J. Park, and V. Koltun, “Fully convolutional geometric features,” in *Proceedings of the IEEE/CVF International Conference on Computer Vision*, 2019, pp. 8958–8966.
- [11] H. Thomas, C. R. Qi, J.-E. Deschaut, B. Marcotegui, F. Goulette, and L. J. Guibas, “Kpconv: Flexible and deformable convolution for point clouds,” in *Proceedings of the IEEE/CVF international conference on computer vision*, 2019, pp. 6411–6420.
- [12] S. Huang, Z. Gojcic, M. Usvyatsov, A. Wieser, and K. Schindler, “Predator: Registration of 3d point clouds with low overlap,” in *Proceedings of the IEEE/CVF Conference on computer vision and pattern recognition*, 2021, pp. 4267–4276.
- [13] H. Yu, F. Li, M. Saleh, B. Busam, and S. Ilic, “Cofinet: Reliable coarse-to-fine correspondences for robust pointcloud registration,” *Advances in Neural Information Processing Systems*, vol. 34, pp. 23 872–23 884, 2021.
- [14] Z. Qin, H. Yu, C. Wang, Y. Guo, Y. Peng, and K. Xu, “Geometric transformer for fast and robust point cloud registration,” in *Proceedings of the IEEE/CVF Conference on Computer Vision and Pattern Recognition*, 2022, pp. 11 143–11 152.
- [15] Y. Li and T. Harada, “Lepard: Learning partial point cloud matching in rigid and deformable scenes,” in *Proceedings of the IEEE/CVF Conference on Computer Vision and Pattern Recognition*, 2022, pp. 5554–5564.
- [16] J. Lee, S. Kim, M. Cho, and J. Park, “Deep hough voting for robust global registration,” in *Proceedings of the IEEE/CVF International Conference on Computer Vision*, 2021, pp. 15 994–16 003.
- [17] X. Bai, Z. Luo, L. Zhou, H. Chen, L. Li, Z. Hu, H. Fu, and C.-L. Tai, “Pointdsc: Robust point cloud registration using deep spatial consistency,” in *Proceedings of the IEEE/CVF Conference on Computer Vision and Pattern Recognition*, 2021, pp. 15 859–15 869.
- [18] G. Mei, X. Huang, L. Yu, J. Zhang, and M. Bennamoun, “Cotreg: Coupled optimal transport based point cloud registration,” *arXiv preprint arXiv:2112.14381*, 2021.
- [19] Y. Shen, L. Hui, H. Jiang, J. Xie, and J. Yang, “Reliable inlier evaluation for unsupervised point cloud registration,” *arXiv preprint arXiv:2202.11292*, 2022.
- [20] H. Jiang, Y. Shen, J. Xie, J. Li, J. Qian, and J. Yang, “Sampling network guided cross-entropy method for unsupervised point cloud registration,” in *Proceedings of the IEEE/CVF International Conference on Computer Vision*, 2021, pp. 6128–6137.
- [21] H. Wang, Y. Liu, Z. Dong, W. Wang, and B. Yang, “You only hypothesize once: Point cloud registration with rotation-equivariant descriptors,” *arXiv preprint arXiv:2109.00182*, 2021.
- [22] Z. J. Yew and G. H. Lee, “Regtr: End-to-end point cloud correspondences with transformers,” in *Proceedings of the IEEE/CVF Conference on Computer Vision and Pattern Recognition*, 2022, pp. 6677–6686.
- [23] A. Vaswani, N. Shazeer, N. Parmar, J. Uszkoreit, L. Jones, A. N. Gomez, Ł. Kaiser, and I. Polosukhin, “Attention is all you need,” *Advances in neural information processing systems*, vol. 30, 2017.
- [24] F. Zhou and F. De la Torre, “Factorized graph matching,” *IEEE transactions on pattern analysis and machine intelligence*, vol. 38, no. 9, pp. 1774–1789, 2015.
- [25] Q. Gao, F. Wang, N. Xue, J.-G. Yu, and G.-S. Xia, “Deep graph matching under quadratic constraint,” in *Proceedings of the IEEE/CVF Conference on Computer Vision and Pattern Recognition*, 2021, pp. 5069–5078.
- [26] G. Peyré, M. Cuturi, and J. Solomon, “Gromov-wasserstein averaging of kernel and distance matrices,” in *International Conference on Machine Learning*. PMLR, 2016, pp. 2664–2672.
- [27] H. Xu, D. Luo, H. Zha, and L. C. Duke, “Gromov-wasserstein learning for graph matching and node embedding,” in *International conference on machine learning*. PMLR, 2019, pp. 6932–6941.



- [28] W. Liu, C. Zhang, J. Xie, Z. Shen, H. Qian, and N. Zheng, "Partial gromov-wasserstein learning for partial graph matching," *arXiv preprint arXiv:2012.01252*, 2020.
- [29] Y. Xie, X. Wang, R. Wang, and H. Zha, "A fast proximal point method for computing exact wasserstein distance," in *Uncertainty in artificial intelligence*. PMLR, 2020, pp. 433–453.
- [30] K. Nguyen, D. Nguyen, T. Pham, N. Ho *et al.*, "Improving minibatch optimal transport via partial transportation," in *International Conference on Machine Learning*. PMLR, 2022, pp. 16656–16690.
- [31] P. J. Besl and N. D. McKay, "Method for registration of 3-d shapes," in *Sensor fusion IV: control paradigms and data structures*, vol. 1611. Spie, 1992, pp. 586–606.
- [32] J. Yang, H. Li, and Y. Jia, "Go-icp: Solving 3d registration efficiently and globally optimally," in *Proceedings of the IEEE International Conference on Computer Vision*, 2013, pp. 1457–1464.
- [33] Q.-Y. Zhou, J. Park, and V. Koltun, "Fast global registration," in *European conference on computer vision*. Springer, 2016, pp. 766–782.
- [34] A. Zeng, S. Song, M. Nießner, M. Fisher, J. Xiao, and T. Funkhouser, "3dmatch: Learning local geometric descriptors from rgb-d reconstructions," in *Proceedings of the IEEE conference on computer vision and pattern recognition*, 2017, pp. 1802–1811.
- [35] H. Deng, T. Birdal, and S. Ilic, "Ppfnet: Global context aware local features for robust 3d point matching," in *Proceedings of the IEEE conference on computer vision and pattern recognition*, 2018, pp. 195–205.
- [36] H. Deng, T. Birdal, and S. Ilic, "Ppf-foldnet: Unsupervised learning of rotation invariant 3d local descriptors," in *Proceedings of the European Conference on Computer Vision (ECCV)*, 2018, pp. 602–618.
- [37] Y. Zhao, T. Birdal, H. Deng, and F. Tombari, "3d point capsule networks," in *Proceedings of the IEEE/CVF Conference on Computer Vision and Pattern Recognition*, 2019, pp. 1009–1018.
- [38] M. Cuturi, "Sinkhorn distances: Lightspeed computation of optimal transport," *Advances in neural information processing systems*, vol. 26, 2013.
- [39] K. Fu, S. Liu, X. Luo, and M. Wang, "Robust point cloud registration framework based on deep graph matching," in *Proceedings of the IEEE/CVF Conference on Computer Vision and Pattern Recognition*, 2021, pp. 8893–8902.
- [40] H. W. Kuhn, "The hungarian method for the assignment problem," *Naval research logistics quarterly*, vol. 2, no. 1-2, pp. 83–97, 1955.
- [41] C. Choy, W. Dong, and V. Koltun, "Deep global registration," in *Proceedings of the IEEE/CVF conference on computer vision and pattern recognition*, 2020, pp. 2514–2523.
- [42] G. D. Pais, S. Ramalingam, V. M. Govindu, J. C. Nascimento, R. Chellappa, and P. Miraldo, "3dregnet: A deep neural network for 3d point registration," in *Proceedings of the IEEE/CVF conference on computer vision and pattern recognition*, 2020, pp. 7193–7203.
- [43] Y. Wang, Y. Sun, Z. Liu, S. E. Sarma, M. M. Bronstein, and J. M. Solomon, "Dynamic graph cnn for learning on point clouds," *Acm Transactions On Graphics (tog)*, vol. 38, no. 5, pp. 1–12, 2019.
- [44] B. Amos and D. Yarats, "The differentiable cross-entropy method," in *International Conference on Machine Learning*. PMLR, 2020, pp. 291–302.
- [45] C. R. Qi, O. Litany, K. He, and L. J. Guibas, "Deep hough voting for 3d object detection in point clouds," in *proceedings of the IEEE/CVF International Conference on Computer Vision*, 2019, pp. 9277–9286.
- [46] R. Wang, J. Yan, and X. Yang, "Neural graph matching network: Learning lawler's quadratic assignment problem with extension to hypergraph and multiple-graph matching," *IEEE Transactions on Pattern Analysis and Machine Intelligence*, 2021.
- [47] R. Zass and A. Shashua, "Probabilistic graph and hypergraph matching," in *2008 IEEE Conference on Computer Vision and Pattern Recognition*. IEEE, 2008, pp. 1–8.
- [48] T. Vayer, L. Chapel, R. Flamary, R. Tavenard, and N. Courty, "Fused gromov-wasserstein distance for structured objects: theoretical foundations and mathematical properties," *arXiv preprint arXiv:1811.02834*, 2018.
- [49] V. Titouan, N. Courty, R. Tavenard, and R. Flamary, "Optimal transport for structured data with application on graphs," in *International Conference on Machine Learning*. PMLR, 2019, pp. 6275–6284.
- [50] E. Grave, A. Joulin, and Q. Berthet, "Unsupervised alignment of embeddings with wasserstein procrustes," in *The 22nd International Conference on Artificial Intelligence and Statistics*. PMLR, 2019, pp. 1880–1890.
- [51] D. Alvarez-Melis, S. Jegelka, and T. S. Jaakkola, "Towards optimal transport with global invariances," in *The 22nd International Conference on Artificial Intelligence and Statistics*. PMLR, 2019, pp. 1870–1879.
- [52] Z. Shen, J. Feydy, P. Liu, A. H. Curiale, R. San Jose Estepar, R. San Jose Estepar, and M. Niethammer, "Accurate point cloud registration with robust optimal transport," *Advances in Neural Information Processing Systems*, vol. 34, pp. 5373–5389, 2021.
- [53] M. Eisenberger, A. Toker, L. Leal-Taixé, and D. Cremers, "Deep shells: Unsupervised shape correspondence with optimal transport," *Advances in Neural information processing systems*, vol. 33, pp. 10491–10502, 2020.
- [54] M. Mandat, D. Cohen-Steiner, L. Kobbelt, P. Alliez, and M. Desbrun, "Variance-minimizing transport plans for inter-surface mapping," *ACM Transactions on Graphics (ToG)*, vol. 36, no. 4, pp. 1–14, 2017.
- [55] M. Frank and P. Wolfe, "An algorithm for quadratic programming," *Naval research logistics quarterly*, vol. 3, no. 1-2, pp. 95–110, 1956.
- [56] M. Zaslavskiy, F. Bach, and J.-P. Vert, "A path following algorithm for the graph matching problem," *IEEE Transactions on Pattern Analysis and Machine Intelligence*, vol. 31, no. 12, pp. 2227–2242, 2008.
- [57] K. Fatras, Y. Zine, R. Flamary, R. Gribonval, and N. Courty, "Learning with minibatch wasserstein: asymptotic and gradient properties," *arXiv preprint arXiv:1910.04091*, 2019.
- [58] K. Fatras, T. Séjourné, R. Flamary, and N. Courty, "Unbalanced minibatch optimal transport; applications to domain adaptation," in *International Conference on Machine Learning*. PMLR, 2021, pp. 3186–3197.
- [59] Z. Chen, H. Chen, L. Gong, X. Yan, J. Wang, Y. Guo, J. Qin, and M. Wei, "Utopic: Uncertainty-aware overlap prediction network for partial point cloud registration," *arXiv preprint arXiv:2208.02712*, 2022.
- [60] J.-D. Benamou, G. Carlier, M. Cuturi, L. Nenna, and G. Peyré, "Iterative bregman projections for regularized transportation problems," *SIAM Journal on Scientific Computing*, vol. 37, no. 2, pp. A1111–A1138, 2015.
- [61] R. L. Dykstra, "An algorithm for restricted least squares regression," *Journal of the American Statistical Association*, vol. 78, no. 384, pp. 837–842, 1983.
- [62] K. Pham, K. Le, N. Ho, T. Pham, and H. Bui, "On unbalanced optimal transport: An analysis of sinkhorn algorithm," in *International Conference on Machine Learning*. PMLR, 2020, pp. 7673–7682.
- [63] A. Geiger, P. Lenz, C. Stiller, and R. Urtasun, "Vision meets robotics: The kitti dataset," *The International Journal of Robotics Research*, vol. 32, no. 11, pp. 1231–1237, 2013.
- [64] A. Paszke, S. Gross, F. Massa, A. Lerer, J. Bradbury, G. Chanan, T. Killeen, Z. Lin, N. Gimelshein, L. Antiga *et al.*, "Pytorch: An imperative style, high-performance deep learning library," *Advances in neural information processing systems*, vol. 32, 2019.
- [65] Z. J. Yew and G. H. Lee, "3dfeat-net: Weakly supervised local 3d features for point cloud registration," in *Proceedings of the European conference on computer vision (ECCV)*, 2018, pp. 607–623.